Synthesis of Air-Stable CdSe/ZnS Core-Shell Nanoplatelets with Tunable Emission Wavelength – Supporting Information

Anatolii Polovitsyn,[a,b] Zhiya Dang,[a] José L. Movilla,[c] Beatriz Martín-García,[a] Ali Hossain Khan,[a] Guillaume H.V. Bertrand,[a] Rosaria Brescia[a] and Iwan Moreels[a,*]

[a] Istituto Italiano di Tecnologia, via Morego 30, 16163 Genova, Italy
[b] Dipartimento di Fisica, Università di Genova, Via Dodecaneso 33, 16146 Genova, Italy
[c] Departamento de Educación, Universitat Jaume I, Av. Vicent Sos Baynat s/n, 12071 Castellón, Spain

*iwan.moreels@iit.it

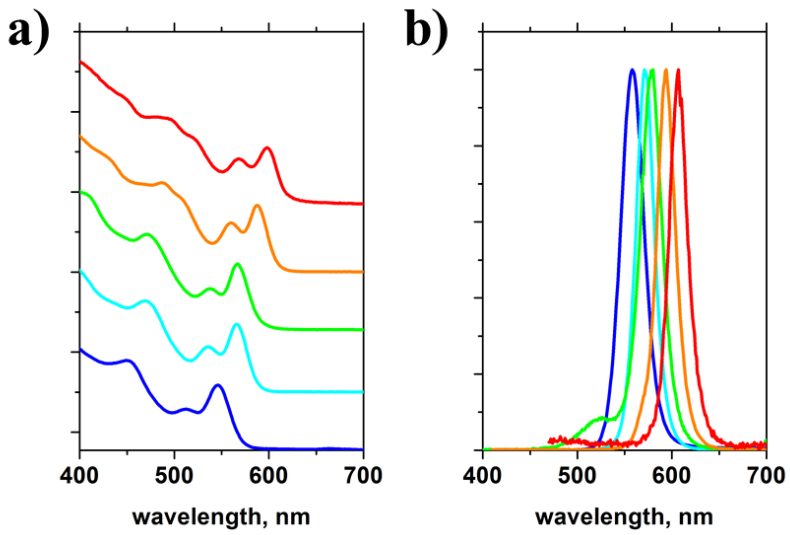

Figure S1. (a) Absorbance and (b) photoluminescence spectra for CdSe wurtzite quantum dots with different diameter. The full width at half maximum of the emission peak ranges from 22 nm to 30 nm.

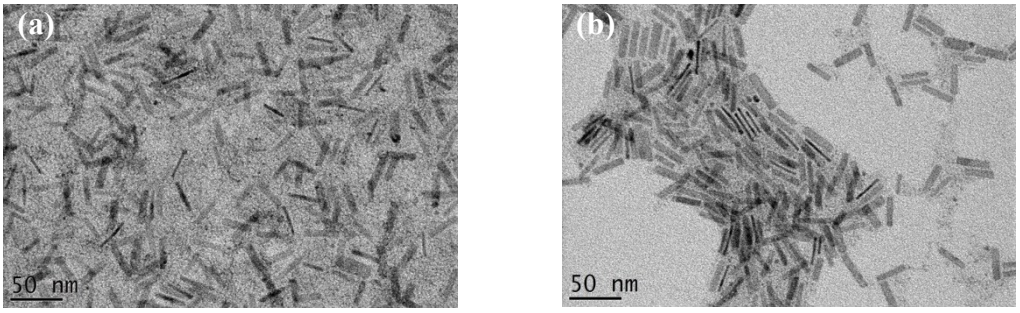

Figure S2. (a) TEM image of an NPL sample precipitated using methanol and showing a background of small clusters. (b) TEM image of the NPLs precipitated using n-isopropanol.

Theoretical outline

The Hamiltonian for the ground-state exciton X^0 in the NPLs reads

$$\hat{H}_{X^0} = \sum_{i=e,h}\{\hat{T}_i + V_i^{pot} + V_i^{self}\} + V_{e-h}^{Coul} \quad \text{(S1)}$$

where $\hat{T}_i$, V_i^{pot}, and V_i^{self} stand for the kinetic energy operator, the quantum confinement potential due to the band offsets, and the self-polarization potential owing to the interaction of the charge carrier *i* (electron or hole) with its own image charges, respectively. Finally, V_{e-h}^{coul} is the Coulomb interaction potential between the electron and hole, which includes the image charge contribution coming from dielectric contrast.

We employed the following trial function to obtain a variational approach for solving the Hamiltonian Eq. (S1):

$$\Psi(\mathrm{r}_e, \mathrm{r}_h) = N\, c(\mathrm{r}_e)c(\mathrm{r}_h)\, e^{-\alpha\,[(x_e-x_h)^2+(y_e-y_h)^2]} \quad \text{(S2)}$$

N is a normalization factor, $c(\mathrm{r}_{e/h})$ is the ground-state wave function of the corresponding 3D effective mass, single-particle Schrödinger equation, and α is the variational parameter yielding a minimum value of

$$\langle \Psi(\mathrm{r}_e, \mathrm{r}_h) | \hat{H}_{X^0} | \Psi(\mathrm{r}_e, \mathrm{r}_h) \rangle \quad \text{(S3)}$$

As can be observed, the trial function Eq. (S2) takes only into account the in-plane (*x, y*) electron-hole correlation. The reason for this simplification is the extremely strong quantum confinement of both particles in the transversal (*z*) direction, which renders them insensitive to Coulomb effects in this direction. For the same reason, we applied the adiabatic approximation to describe the single particle (electron and hole) states, $c(\mathrm{r}_{e/h})$. Assuming infinite confinement barriers in *x* and *y*, these read, in atomic units, a.u.:

$$c(\mathrm{r}_i) = N_i \cos(k_x x_i) \cos(k_y y_i)\, \theta_i(z_i) \quad \text{(S4)}$$

$k_x = \pi/L_x$ and $k_y = \pi/L_y$, with L_x and L_y the in-plane dimensions of the CdSe NPLs. The transversal (*z*) components of the electron and hole wave functions are represented in Eq. (S4) by θ_i. In order to include the possible exciton tunneling into the ZnS shell, the CdSe/ZnS interfaces in the *z*-coordinate were modeled as step-like potentials reproducing the corresponding band offsets. Infinite barriers where considered for the NPL – ligands interface, according to results supporting the large offsets involved.[1]

The $\theta_i(z_i)$ components of the single-particle wave functions were obtained numerically by means of a finite differences scheme. We considered the different electron and hole effective masses in the CdSe core and the ZnS shell. To account for the mass mismatch, we employed the kinetic energy operator proposed by BenDaniel and Duke:[2]

$$\hat{T} = -\frac{1}{2}\frac{d}{dz}\frac{1}{m_z^*(z)}\frac{d}{dz} \quad \text{(S5)}$$

This preserves the Hermitian condition of the Hamiltonian. The source of inaccuracy arising from the δ-function nature of dm_z^*/dz was overcome by following a proper discretization of the kinetic energy operator.[3,4]

As for dielectric effects, in the current calculations we focused on the NPL – ligands dielectric interfaces along the transversal direction, as these constitute the unique source of dielectric confinement capable of influencing the exciton energy and dynamics.[5,6] The corresponding V_i^{self} and V_{e-h}^{coul} expressions read, in a.u.:[7]

$$V_i^{self}(\mathrm{r}_i) = \sum_{n=-\infty}^{-1} \frac{q_n}{2\varepsilon_{NPL}|z_i-(-1)^n z_i+nL_d|} + \sum_{n=1}^{\infty} \frac{q_n}{2\varepsilon_{NPL}|z_i-(-1)^n z_i+nL_d|}, \quad \text{(S6)}$$

$$V_{e-h}^{Coul}(\mathrm{r}_e, \mathrm{r}_h) = \sum_{n=-\infty}^{\infty} \frac{q_n}{\varepsilon_{NPL}\sqrt{(x_e-x_h)^2+(y_e-y_h)^2+[z_e-(-1)^n z_h+nL_d]^2}}, \quad \text{(S7)}$$

$q_n = \left(\frac{\varepsilon_{NPL}-\varepsilon_{\mathrm{lig}}}{\varepsilon_{NPL}+\varepsilon_{\mathrm{lig}}}\right)^{|n|}$, ε_{NPL} ($\varepsilon_{\mathrm{lig}}$) is the dielectric constant of the NPL (ligands), and L_d is the thickness of the NPL including the ZnS shell.

To evaluate the Coulomb integral appearing in Eq. (S3), we use the following representation of the inverse electron-hole distance:[8]

$$\frac{1}{|\mathrm{r}_e-\mathrm{r}_h|} = \pi^{-1/2} \int_0^{\infty} dt\, t^{-1/2}\, e^{-t\,(\mathrm{r}_e-\mathrm{r}_h)^2}. \quad \text{(S8)}$$

Thus, the Coulomb interaction potential can be written in our case as:

$$V_{e-h}^{Coul}(\mathrm{r}_e, \mathrm{r}_h) = \frac{1}{\varepsilon_{NPL}\sqrt{\pi}} \sum_{n=-\infty}^{\infty} q_n \int_0^{\infty} dt\, t^{-\frac{1}{2}}\, e^{-t\,(\mathrm{x}_e-\mathrm{x}_h)^2} e^{-t\,(\mathrm{y}_e-\mathrm{y}_h)^2} e^{-t\,(z_e-(-1)^n z_h+nL_d)^2} \quad \text{(S9)}$$

This expression allows us to integrate each dimension independently, turning the sextuple Coulomb integral into three double integrals (two (in *x* and *y*) of which can be solved analytically) plus a final integration in *t* which is done numerically. The set of parameters employed in the calculations is summarized in the **Table S1**.

Once obtained the optimized exciton wave functions $\Psi(\mathrm{r}_e, \mathrm{r}_h)$, the corresponding electron-hole overlaps, mean in-plane electron-hole distances and charge density distributions (average and conditional) were calculated as

$$S_{e-h}^2 = |\int \Psi(\mathrm{r}, \mathrm{r}) d\mathrm{r}|^2,$$

$$\bar{d}_{e-h} = |\langle\Psi|(x_e - x_h)^2 + (y_e - y_h)^2|\Psi\rangle|^{\frac{1}{2}},$$

$$\rho_i(x_i, y_i) = \int_{x_j, y_j}^{z_e, z_h} |\Psi(\mathrm{r}_e, \mathrm{r}_h)|^2,$$

$$\rho_i(x_i, y_i; x_j^0, y_j^0) = \int_{z_i, z_j} \left|\Psi(x_i, y_i, z_i; x_j^0, y_j^0, z_j)\right|^2, \quad \text{(S10)}$$

$\rho_i(x_i, y_i)$ equals the averaged charge density distribution of the particle *i* and $\rho_i(x_i, y_i; x_j^0, y_j^0)$ is the charge density distribution of the particle *i* when the in-plane location of the particle *j* is fixed at (x_j^0, y_j^0).

Table S1. Set of parameters employed in the calculations.

CdSe core size		Length (nm)	37
		Width (nm)	8
		Thickness (ML)	4.5
Lattice parameters		a_{CdSe} (Å)	6.05
		a_{ZnS} (Å)	5.32
Band offsets		Conduction (eV)	1.44 [a]
		Valence (eV)	0.6 [a]
Dielectric constants		ε_{NPL}	8 [b]
		ε_{lig}	2
Transversal (z) effective masses	CdSe	$m^*_{e,z}$	0.12 [b]
		$m^*_{hh,z}$	0.9 [b]
	ZnS	$m^*_{e,z}$	0.28 [c]
		$m^*_{hh,z}$	1.76 [c]
In-plane (xy) effective masses		$m^*_{e,\parallel}$	0.27 [d]
		$m^*_{hh,\parallel}$	0.45 [d]

a. From Ref. [9]
b. From Ref. [10]
c. From Ref. [11]
d. From Ref. [1]

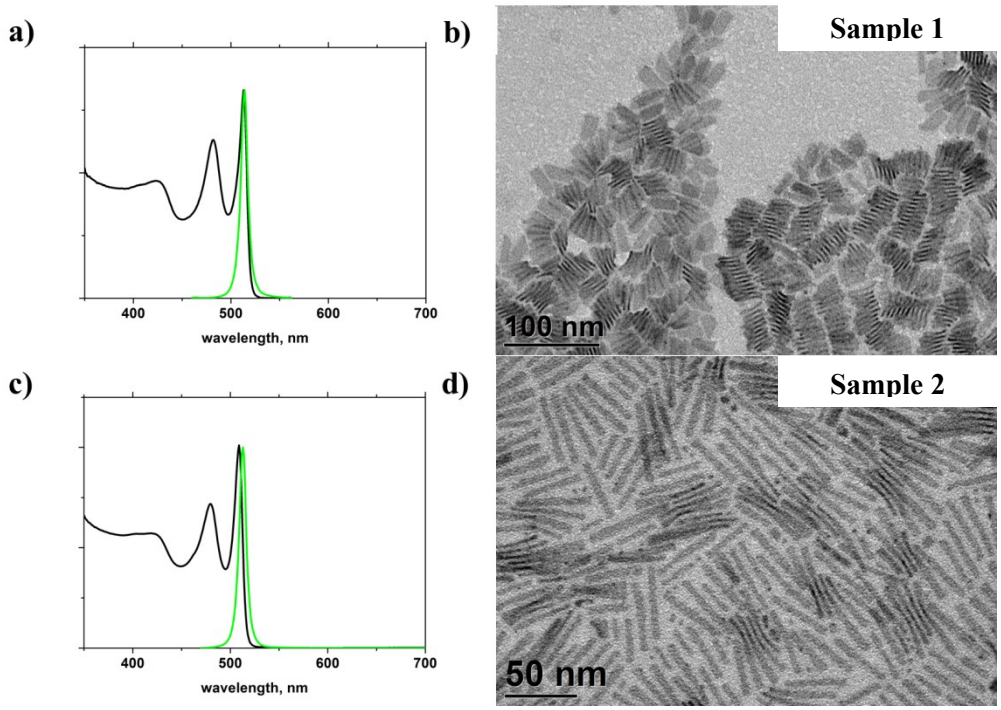

Figure S3. (a,c) Absorbance (black) and photoluminescence (green) spectra for typical CdSe NPLs used in this work. (b,d) Corresponding TEM images of the CdSe NPLs.

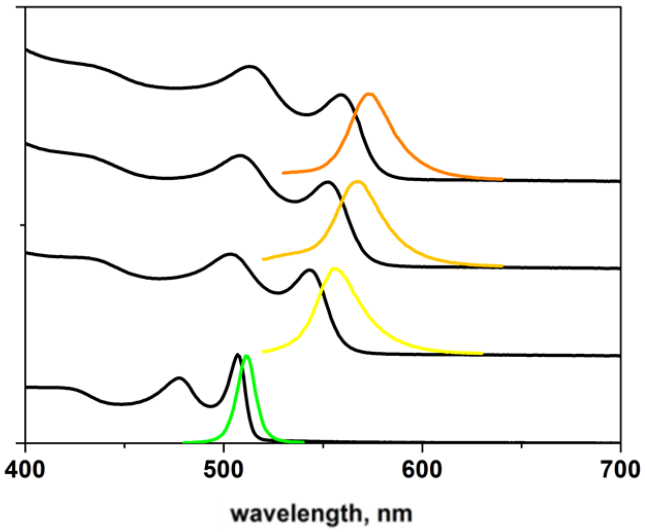

Figure S4. Absorbance and photoluminescence spectra for CdSe/ZnS core/shell NPLs samples with different shell thickness using $ZnCl_2$ and CS_2 as ZnS precursors, synthesized at 110 ^{o}C in toluene as a solvent.

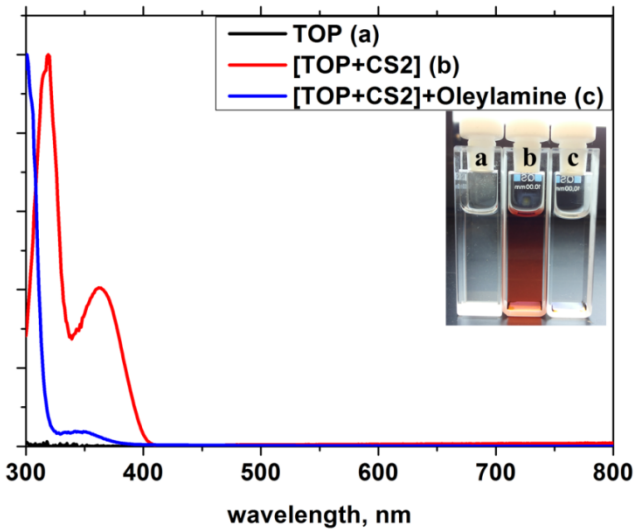

Figure S5. Absorbance spectra of TOP, and the TOP-CS_2 complex before and after addition of oleylamine. Spectra collected as 0.1 mM solutions in toluene.

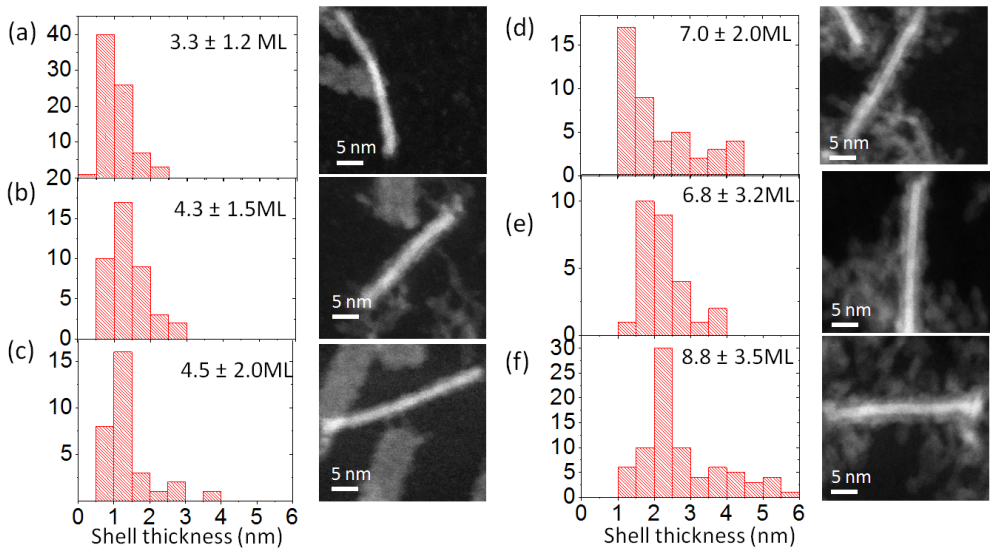

Figure S6. Typical HAADF-STEM images of different CdSe/ZnS NPLs (target thickness of 5ML (a), 7ML (b), 9ML (c), 11ML (d), 13ML (e), 15ML (f)), synthesized from 35.4 nm by 5.9 nm CdSe core NPLs (sample 3) in DCB at 150 °C. The shell growth is evaluated by measuring the shell thickness of 8-26 particles, at three to four positions for each particle. The resulting histograms yield the average shell thickness and standard deviation. Data are also plotted in the main text, Figure 6, together with the red shift of the emission peak.

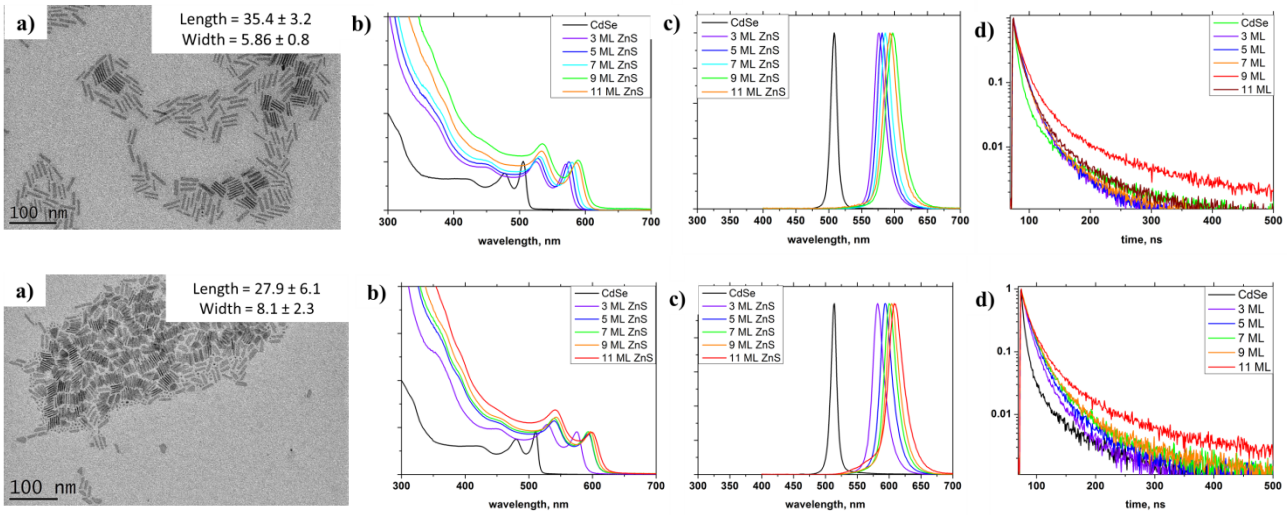

Figure S7. Top: (a) Typical TEM image of the CdSe core NPLs (sample 3) used to prepare a series of CdSe/ZnS core/shell NPLs. (b-d) Series of absorbance spectra (b), photoluminescence spectra (c) and time-resolved fluorescence decay traces (d) of core/shell NPLs.
Bottom: We repeated the optical spectroscopy on a sample with different dimensions (sample 4). (a) Typical TEM image of the CdSe core NPLs used to prepare a series of CdSe/ZnS core/shell NPLs. (b-d) Series of absorbance spectra (d), photoluminescence spectra (c) and time-resolved fluorescence decay traces (d) of core/shell NPLs, with targeted shell thickness up to 11ML.

Table S2. PL quantum efficiencies and amplitude-weighted average lifetime (obtained from a multiexponential fit to the decay traces in Figure S7) for CdSe/ZnS NPLs with different targeted shell thickness.

Core sample	Solvent	ZnS shell thickness, ML	PL, nm	PL QE, λ_{ex} 450 nm	τ_{avg}, ns
Sample 3		0	508.2	37	7.1
	DCB	3	576.3	62	10.6
	DCB	5	581.1	63	10.9
	DCB	7	586.2	48	10.3
	DCB	9	597.4	13	13.7
	DCB	11	593.5	10	9.9
Sample 4		0	513.6	29	5.7
	DCB	3	582.2	64	11.8
	DCB	5	594.1	59	13.8
	DCB	7	600.6	55	14.8
	DCB	9	604.2	49	15.1
	DCB	11	609.1	12	16.9

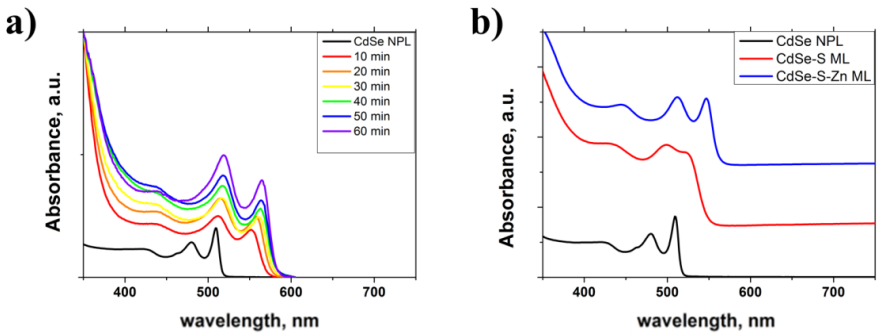

Figure S8. (a) Absorbance spectra of a time-resolved study of ZnS shell growth, aliquots were taken each 10 min. (b) Absorbance spectra for CdSe NPLs after depositing a single sulfur and zinc layer by c-ALD at room temperature.

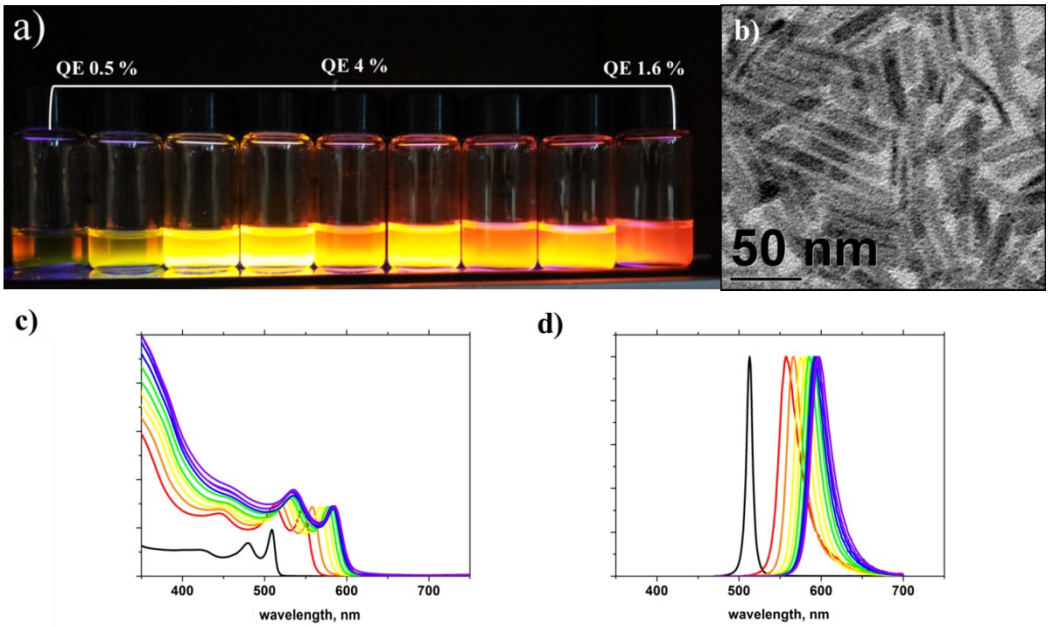

Figure S9. (a) Photo image of CdSe/ZnS core/shell NPLs with increasing shell thickness, deposited in monolayer steps using c-ALD. The PL QE of the samples is indicated above the vials. (b) TEM image for CdSe/ZnS NPLs with 10 ML of ZnS shell. (c-d) Absorbance and photoluminescence spectra, showing the continuous red shift as the shell thickness increases (the black line corresponds to CdSe core-only NPLs).

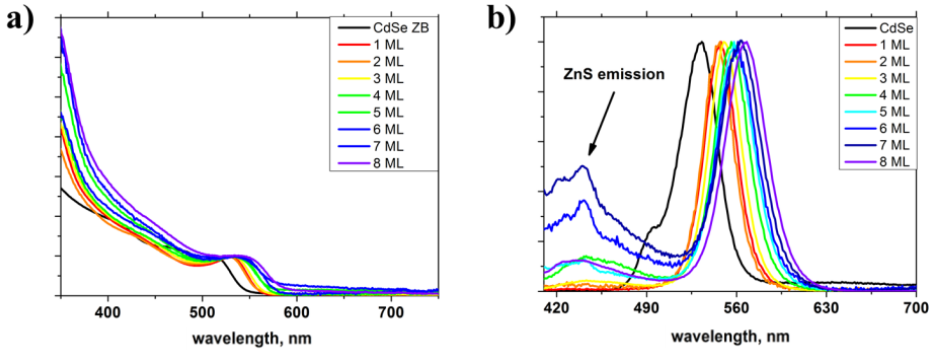

Figure S10. (a) Absorbance and (b) PL spectra for CdSe/ZnS core/shell QDs. The ZnS was deposited in 1 ML steps by c-ALD at room temperature. The additional band at shorter wavelengths is possibly due to trap-state emission in the ZnS shell.

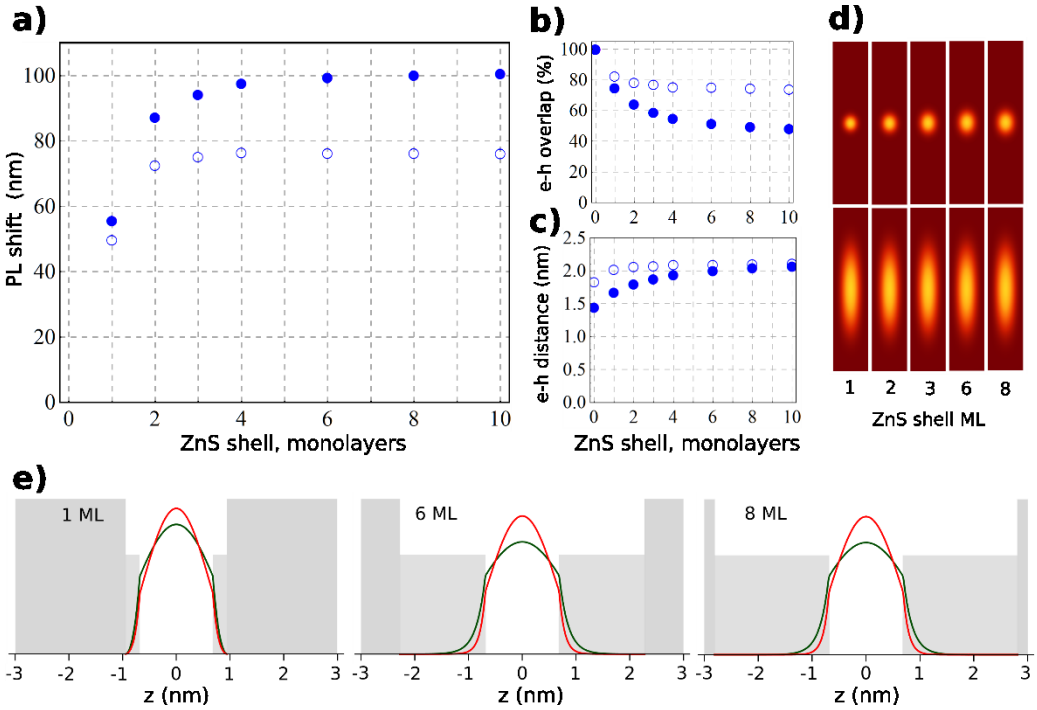

Figure S11. (a) Calculated PL shifts, (b) electron-hole overlaps, and (c) mean electron-hole in-plane distances as a function of the thickness of a ZnS shell grown on a 37x8 nm CdSe NPL 4.5 ML thick. Filled (open) symbols correspond to calculations including (excluding) the dielectric contrast with the organic ligands and environment. (d) In-plane electron (or hole) charge density distribution for several ZnS shell thicknesses. Lower panels represent average density distributions $\rho_i(x_i, y_i)$. Upper panels represent conditional density distributions $\rho_i(x_i, y_i; x_j^0, y_j^0)$ with $(x_j^0, y_j^0) = (0, 0)$. (e) Transversal profile of the electron (green line) and hole (red line) densities for ZnS shell thicknesses of 1, 6, and 8 ML, showing the exciton leakage into the ZnS shell.

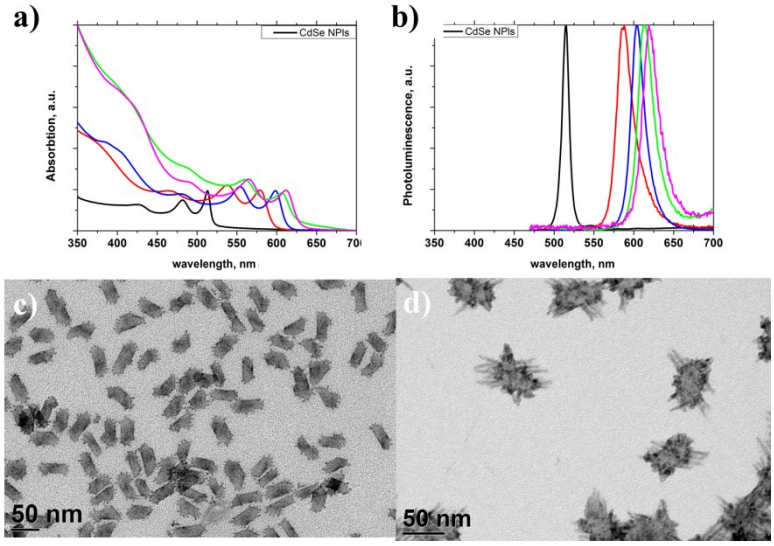

Figure S12. (a) Absorbance, (b) photoluminescence spectra and (c) TEM image for CdS shells deposited using $CdCl_2$ and CS_2. (d) TEM image of CdSe/CdS NPLs synthesized using $CdCl_2$, $Cd(DDTC)_2$ and CS_2.

References

(1) Benchamekh, R.; Gippius, N. A.; Even, J.; Nestoklon, M. O.; Jancu, J.-M.; Ithurria, S.; Dubertret, B.; Efros, A. L.; Voisin, P. Tight-Binding Calculations of Image-Charge Effects in Colloidal Nanoscale Platelets of CdSe. *Phys. Rev. B* **2014**, *89*, 035307.

(2) BenDaniel, D. J.; Duke, C. B. Space-Charge Effects on Electron Tunneling. *Phys. Rev.* **1966**, *152*, 683–692.

(3) Harrison, P.; Valavanis, A. Quantum Wells, Wires and Dots: Theoretical and Computational Physics of Semiconductor Nanostructures, Wiley.

(4) Movilla, J. L.; Planelles, J. Image Charges in Spherical Quantum Dots with an off-Centered Impurity: Algorithm and Numerical Results. *Comput. Phys. Commun.* **2005**, *170*, 144–152.

(5) Rodina, A. V.; Efros, A. L. Effect of Dielectric Confinement on Optical Properties of Colloidal Nanostructures. *J. Exp. Theor. Phys.* **2016**, *122*, 554–566.

(6) Even, J.; Pedesseau, L.; Kepenekian, M. Electronic Surface States and Dielectric Self-Energy Profiles in Colloidal Nanoscale Platelets of CdSe. *Phys. Chem. Chem. Phys.* **2014**, *16*, 25182–25190.

(7) Kumagai, M.; Takagahara, T. Excitonic and Nonlinear-Optical Properties of Dielectric Quantum-Well Structures. *Phys. Rev. B* **1989**, *40*, 12359–12381.

(8) Bryant, G. W. Hydrogenic Impurity States in Quantum-Well Wires: Shape Effects. *Phys. Rev. B* **1985**, *31*, 7812–7818.

(9) Xie, R.; Kolb, U.; Li, J.; Basché, T.; Mews, A. Synthesis and Characterization of Highly Luminescent CdSe−Core CdS/$Zn_{0.5}Cd_{0.5}$S/ZnS Multishell Nanocrystals. *J. Am. Chem. Soc.* **2005**, *127*, 7480–7488.

(10) Kim, Y. D.; Klein, M. V.; Ren, S. F.; Chang, Y. C.; Luo, H.; Samarth, N.; Furdyna, J. K. Optical Properties of Zinc-Blende CdSe and ZnxCd1-xSe Films Grown on GaAs. *Phys. Rev. B* **1994**, *49*, 7262–7270.

(11) Lawaetz, P. Valence-Band Parameters in Cubic Semiconductors. *Phys. Rev. B* **1971**, *4*, 3460–3467.